POPULAR SUMMARY

Ice-Crystal Fallstreaks from Supercooled Liquid Water Parent Clouds

James R. Campbell
Science Systems & Applications, Inc., Greenbelt, Maryland

David OíC. Starr, Ellsworth J. Welton, James D. Spinhirne
NASA Goddard Space Flight Center, Greenbelt, MD

Richard A. Ferrare
NASA Langley Research Center, Hampton, VA

Submitted to *Monthly Weather Review*
September 2003

On 31 December 2001, ice-crystal fallstreaks (e.g., cirrus uncinus, or colloquially "Mare's Tails") from supercooled liquid water parent clouds were observed by ground-based lidars pointed vertically from the Atmospheric Radiation Measurement Southern Great Plains (SGP) facility near Lamont, Oklahoma. The incidence of liquid phase cloud with apparent ice-phase precipitation is investigated. Scenarios for mixed-phase particle nucleation, and fallstreak formation and sustenance are discussed. The observations are unique in the context of the historical reverence given to the commonly observed cirrus uncinus fallstreak (wholly ice) versus this seemingly contradictory coincidence of liquid water begetting ice-crystal streaks. In contrast to the more common observations of glaciation of liquid phase altocumulus or altostratus clouds leading to erosion of the parent cloud and development of a cloud "hole" and persistent ice fallstreak below it, we find that the liquid-phase parent cloud persists in this case, a finding more common in the arctic than in middle latitudes as here.

Ice-Crystal Fallstreaks from Supercooled Liquid Water Parent Clouds

James R. Campbell*
Science Systems & Applications, Inc., Greenbelt, Maryland

David O'C. Starr, Ellsworth J. Welton, James D. Spinhirne
NASA Goddard Space Flight Center, Greenbelt, MD

Richard A. Ferrare
NASA Langley Research Center, Hampton, VA

Submitted to Monthly Weather Review

* Corresponding author address: 10210 Greenbelt Rd, Suite 600, Lanham, MD, USA, 20706. E-mail: campbell@virl.gsfc.nasa.gov

ABSTRACT

On 31 December 2001, ice-crystal fallstreaks (e.g., cirrus uncinus, or colloquially "Mare's Tails") from supercooled liquid water parent clouds were observed by ground-based lidars pointed vertically from the Atmospheric Radiation Measurement Southern Great Plains (SGP) facility near Lamont, Oklahoma. The incidence of liquid phase cloud with apparent ice-phase precipitation is investigated. Scenarios for mixed-phase particle nucleation, and fallstreak formation and sustenance are discussed. The observations are unique in the context of the historical reverence given to the commonly observed cirrus uncinus fallstreak (wholly ice) versus this seemingly contradictory coincidence of liquid water begetting ice-crystal streaks.

1. Introduction

To even the most casual sky observer, cirrus uncinus fallstreaks (colloquially referred to as "Mare's Tails") can produce spectacular visual displays. It would be difficult to reference any consequential cloud atlas that does not at least briefly consider such formations. Recently Atlas (2001), relying on a single photograph, describes an analogous situation where uncinus-like (i.e. ice-phase) fallstreaks are produced by supercooled liquid water-phase (SLW) generating cells (the nature of the parent cloud is not distinctly classified). This scenario is novel in that it represents an atmospheric paradox; that is, liquid-phase cloud begetting apparent ice-phase precipitation. The author was limited wholly to the single still, which was taken in haste so as to capture the moment. No notes were taken, and as such the date of the event was not logged so that no further investigation of the thermodynamic or synoptic environment could be supplemented. The works of Heymsfield (1975a-c) and Ludlam (1948, 1956, and 1980) provided a dynamic framework of generic cirrus uncinus generating heads and fallstreaks from which to reconcile what mechanisms were at work within the clouds.

The current lead author was already familiar with the Atlas (2001) article when, during routine processing of micropulse lidar (Campbell et al., 2002; MPL, 0.523 μm) data from the Atmospheric Radiation Measurement program (Stokes and Schwartz, 1994) Southern Great Plains Cloud and Radiation Testbed (SGP, CART) central facility (CF), he came across observations collected during the early hours (UTC) of 31 December 2001. The sky conditions were immediately reminiscent of those captured photographically in Atlas (2001). These data are shown in Fig. 1, plotted versus altitude to 8.0 km, between 0000 – 1200 UTC (1800 30 December – 0600 local Central Standard Time; CST). Beginning at

about 0430 UTC (2230 CST), ice-crystal fallstreaks were detected by the lidar emanating downward from a layer at an altitude of about 6.0 km above ground level (AGL). Shortly afterward, additional streaks were observed falling from a parent SLW cloud at 6.0 km AGL, and then from parent clouds at about 5.4 km AGL after 0615 UTC. The depths of the fallstreaks were significant, ranging from 0.5 to 1.5 km below cloud base. Our initial discrimination of parent cloud phase is based on the level of MPL signal attenuation beyond (above) the SLW cloud layers in Fig. 1 (note the "shadowing" of signal above the SLW clouds, indicating the extinguishing of the transmitted pulse energy). Due to enhanced signal cross-sections within liquid-phase clouds, versus those composed of ice, we can be confident to a first-order approximation of this phase attribution. Note that these clouds formed before sunrise such that no ground observers or ground-based passive sky imaging instruments could record the event.

The purpose of this article is to expand upon the discussion of Atlas (2001), and offer a more detailed investigation into the coincidence of liquid-phase parent clouds and ice-phase fallstreaks. Our goal is to more completely characterize the dynamic and thermodynamic mechanisms that were occurring, and explain how SLW droplet growth was able to persist in the presence of appreciable ice nucleation. Additional information from nearby remote sensors operating concurrently at the CF and beyond is supplemented. Although middle tropospheric mixed-phase clouds are well-understood to correspond with glaciating virga, sometimes leading to stable stratiform cirrus clouds or even vice versa (e.g., Sassen 2003), this case was unique in that the parent clouds were persistent, and the fallstreak depths so significant. Had a ground observer been witness to

the event, the sight would have been perplexing, yet every bit comparable to classic cirrus uncinus (wholly ice) displays.

2. Case Evolution

A more robust view of the event comes from data collected simultaneously by the CART Raman Lidar instrument (CARL; 0.355 μm native), collocated with the MPL at the CF (Goldsmith et al., 1999). Measured laser depolarization ratios and signal-derived relative humidities (with respect to liquid water; Turner et al., 2000; 2002) are shown in Figs. 2a-b respectively between 0000 – 1200 UTC. From Fig. 2a, ice-crystal fallstreaks corresponding to the MPL observations are clearly apparent, whereas the parent SLW clouds are not. Spherical water droplets are inefficient in generating significant depolarization of transmitted laser pulses, whereas ice crystals, with irregular shapes, act just the opposite (Sassen 1991). More striking is the nature of the vertical water vapor structure observed during the event. A clear delineation between humid and dry air can be seen along a boundary lowering from 8.0 to 5.0 km AGL between 0200 and 1200 UTC in Fig. 2b. The location of the SLW parent clouds correspond closely to the top of the relatively humid layer at 0600 and afterwards.

A view of the vertical thermodynamic structure comes from rawinsonde profiles shown in Fig. 3. Sondes are launched from the CF (by ARM) at six-hour intervals. Shown here are those for 0000, 0600 and 1200 UTC from the 31st. A sequence of potential temperature profiles (progressively offset 20 K, respectively, with 0000 UTC beginning on the left) detailing isentropic progression is given in Fig. 3a. The relative humidity structure (both liquid and ice based upon temperature; see figure caption) is

shown in Fig. 3b. Figure 4 is an expansion of Figs. 3a-b plotting the 0600 and 1200 temperatures and dewpoints with relative humidities (both liquid and ice) overlaid. The CF is approximately 0.3 km above mean sea level (MSL; note that these units are used with the soundings for vertical scale; the lidar data from Figs. 1 and 2 are AGL). Wind data are not shown, but will be cited as needed. A surface front had recently passed (0000 UTC on the 29th) bringing cold air and snowfall to the region. The elevated cold frontal boundary is located at a height of about 2.0 km MSL corresponding to the inversion (packed isentropes) at that level. Also note the strong nocturnal inversion over the freshly snow-covered surface at 0600 and 1200 UTC. The cold air mass is stably stratified, as is the overlying air. From Fig. 1, the MPL data (and CARL aerosol extinction data; not shown) indicate a denser aerosol layer constrained below approximately 1.0 km AGL with a detached aerosol layer near the 2.0 km AGL level, just above the frontal zone. We conclude that the lower troposphere was effectively decoupled from the middle troposphere while the fallstreak event was occurring.

Other features suggestive of elevated boundaries (packed isentropes) at 0600 UTC are seen near 5.5 km (0.4° C inversion over 0.060 km depth) and 7.0 km MSL (isothermal over 0.150 km depth; Fig. 3a). A less pronounced boundary can also be seen at 6.3 km MSL. All were located earlier at lower heights (i.e., sloped upward in the upwind direction). The lower feature persists through 1200 UTC. Below it, where fallstreaks appeared after 0600 UTC, the stratification is less stable and becomes approximately dry-adiabatic (well mixed) by 1200 UTC. This reflects destabilization due to the vertical distribution of cooling from sublimation in the fallstreaks. Figure 4 shows the cooling to be greatest just below the nearly 2° C inversion at 5.4 km MSL. Below 4.0 km MSL to

the frontal surface, the profiles indicate relatively strong static stability that changes little through the period. Of passing interest is the nearly well mixed stratification found in the upper troposphere, especially at 0000 and 1200 UTC. The moisture observations (Fig. 3b) show a humid layer from about 5.0 km to 7.0 km MSL at 0600 UTC sandwiched between relatively dry layers, in excellent agreement with the CARL observations (Fig. 2b). The region above about 5.4 km MSL dries considerably by 1200 UTC, replaced by a relatively thin layer of high humidity at about 5.3 km (-23° C).

Satellite imagery from Geostationary Operational Environment Satellite (GOES-8) are shown in Fig. 5, specifically from the 10.7 μm infrared channel (a-d) and 6.8 μm upper tropospheric water vapor channel (e-h) for 0000, 0300, 0600 and 0900 UTC, centered around the CART site[1]. A synoptic-scale trough encompassed the eastern two-thirds of the continental United States. At 0600 UTC, maximum wind speeds of 90 kt at 300 mb were occurring along the leeside of the Rocky Mountains reaching into the base of the trough over northern Mexico (not shown). The dry streak across Kansas delineates a short-wave impulse advancing southeastward, which can be seen to gradually phase into the larger trough through the sequence. The SLW/fallstreak complex observed at the CF was associated with a wedge of moisture ahead of this short wave. This is most clearly apparent from the 0300 and 0600 water vapor images (Figs. 4f-g). These mid-level clouds are mid-gray in the IR imagery (Figs. 4a-d) consistent with their temperature. A cold (brighter) upper tropospheric cloud system (i.e., baroclinic leaf) is seen to the southeast of the CF associated with the surface front.

[1] GOES imagery for the ARM Southern Great Plains CART region were obtained via the NASA Langley Atmospheric Sciences Division World Wide Web page at http://www-angler.larc.nasa.gov/armsgp/.

The first fallstreaks emanating from SLW parent cells occurred at about 0600 UTC, with cloud based near the weak 6.3 km MSL boundary (6.0 km AGL in Fig. 1). Temperatures at this height were about -29° C. Data from the 0600 UTC sonde (height MSL) and CARL measurements (height AGL) show three relative humidity peaks (liquid; Fig. 4) with values of 95 percent at 6.3/6.0 km, and other peaks near 5.4/5.1 km (94 percent) and 6.9/6.6 km (88 percent). The peak at 6.3/6.0 km corresponds very well to the location of the thin SLW cloud layer observed around 0600 UTC while the peak at 5.4/5.1 km corresponds to the cloud layer that developed shortly thereafter. By 0900 UTC, the nearly phased dual trough axis passed the CF (Fig. 4h). As the source of induced broad-scale ascent passed fallstreak observations ceased. Moreover, extreme drying (subsidence) occurred at heights (Fig. 2) just above the cloud-forming layer. This drying may possibly have been derived from a stratospheric intrusion upwind of the CF, suggested by the shape in Fig. 2.

There is evidence that this event was not localized. Shown in Fig. 6 are a twelve-hour series of vertical velocity profiles measured by a NOAA 404 MHz Doppler wind profiler located at Vici, Oklahoma[2]. Vici is approximately 150 km west-southwest of the CF. These data are shown from 2100 UTC 30 December to 0900 UTC on the 31st. An area of decent (1.0 m/s and greater) occurred within the 3.0 and 5.5 km AGL layer between 0000 and 0300 UTC. Given the displacement from the CF, it is safe to assume that such conditions likely occurred there no later than 0500 UTC (using simply the minimum 30 kt wind speeds measured just above the boundary layer in each sounding), which corresponds with the commencement of fallstreak observations from the lidars.

---

[2] NOAA Wind Profiler Network data may be obtained from http://www.profiler.noaa.gov

3. Discussion

The ice-crystal fallstreaks and SLW parent clouds were the result of mixed-phase cloud growth, associated with the elevated boundaries at 5.4 and 6.3 km MSL. In the incidence of ice-crystal fallstreaks, what would otherwise have appeared to a ground observer to be cirrus uncinus was actually much closer in nature to altocumulus. Mixed-phase mid-level clouds are well understood to form in areas of lifting and/or cooling and in the presence of elevated inversion boundaries. In this case, the advecting mid-level trough could have been the responsible dynamic trigger. However, we cannot speak conclusively to this. The possibility of post-frontal gravity waves in the middle troposphere as the cause is intriguing as such conditions have been documented previously in the region in similar post-frontal environments (Ralph et al, 1999). Worthington (2002) examines ice-phase fallstreaks associated with breaking gravity waves south of Ireland. One can even glean some periodicity to the parent SLW cloud observations in Fig. 1.

Within the parent clouds it is important to understand how liquid phase growth was sustained, and how SLW droplets were able to grow and subsist despite coinciding ice nucleation. Temperatures were warm relative to the point of homogeneous ice nucleation near –38° C (Sassen and Dodd, 1988) requiring the presence of suitable airborne nuclei to induce freezing/deposition within the saturated air. Scavenging of liquid water as well as the Bergeron-Findeisen effect (governing the offset of saturation vapor pressures between liquid and ice and acting to increase ice particle growth at the expense of liquid droplets) would both have also acted to gradually freeze any condensate. However, those ice particles that formed could only take advantage of favorable in-cloud conditions for a

finite length of time before falling out due to increasing particle size and gravity. Had the ice completely dehydrated the parent cloud layer, a cloud "hole" would have formed, whereby the parent cloud would have been removed. This explains the lack of a parent head with the initial fallstreak seen around 0430 UTC in Fig. 1 (a less distinct streak can also be seen near 0330 UTC). · The fallstreak represents the glaciated remnants of the parent head. In fact, depolarization ratios from the top of this streak are somewhat lower than subsequent streaks. It is possible that a liquid coalescence to the ice-crystals was influencing scattering from those particles just below the condensation/deposition level (i.e., scavenging). The effects of the precursor streaks on the local environment (aside from enhancing sub-cloud relative humidities as discussed above) may have been directly led to the initial SLW parent cloud cell at 6.0 km AGL seen just before 0600 UTC. This could have occurred either from a modification (warming) of ambient air due to latent heat release, or by simple scavenging of available ice nuclei at that level. Either or both would have lessened the significance of ice nucleation relative to that of droplet growth.

Given the temperature inversions at both SLW cloud-generating levels it is conceivable that a variable dominance in phase nucleation could also have been occurring in relation to the temperature gradient within the condensation/deposition layer. That is, greater ice nucleation could have been occurring in the colder air below more dominant condensation in the slightly warmer air above. As such, the effects of scavenging and Bergeron-Findeisen deposition would have also scaled in relative magnitude with height. Although the magnitude of each inversion (< 2° C) would not suggest a large gradient in saturation vapor pressures, the effect of such a scenario would have been duly magnified had available ice nuclei similarly been stratified along the inversion boundary. Though

we cannot speak for certain, such an explanation helps justify the significance of the parent clouds. Attenuation of the MPL signal seen in Fig. 1 intermittently with the SLW parent clouds indicates their optical depths at 0.523 μm to be on the order of 3.0 (Sassen and Cho, 1992). As such, these were otherwise ordinary mid-level clouds (with respect to optical appearance) that showed little effects of dilution from the fallstreaks.

The sub-cloud environment was ideal to sustaining and enhancing the growth of the falling ice-crystals. The layer between 5.0 km MSL and cloud base was effectively saturated with respect to water, and mostly supersaturated with respect to ice (Fig. 4). Each successive streak enhanced and sustained the environment for its successor, thereby creating a small-scale feedback. Linear depolarization rates from Fig. 2b show variable returns with range within the falling streaks. This indicates change to particle shape and size (and perhaps to a lesser degree fall orientation) as they fell further towards ground. Sublimation efficiencies within ice particles falling below cloud base are dependent upon available moisture, and the rate of entrainment of drier air. We believe that the particles likely continued to grow during their fall, though we cannot speak directly to particle number densities, which should otherwise have been conserved before sublimation (Spinhirne et al., 1998). A lack of significant speed and directional wind shear within the fallstreaks apparent from the rawinsondes (not shown) and lidar data was significant. The stacked nature of the event limited entrainment since the fallstreaks were practically falling into their updrafts, as suggested conceptually by Heymsfield (1975b). This further acted to sustain the moisture-rich sub-cloud layer and indirectly aided the enhancement of ice particle lifetimes during their fall.

4. Conclusions

Middle tropospheric clouds (e.g., altocumulus) commonly result from some degree of mixed-phase growth. The observations discussed here represent a significantly anomalous case where such clouds reached equilibrium between liquid droplet growth, glaciating particle nucleation/growth and fallstreak production so that they serendipitously resembled (at least macrophysically) a traditional cirrus uncinus structure. Furthermore, the persistence of these mechanisms, a near-ideal sub-cloud environment and moisture replenishing of the fallstreak layer through continued sublimation combined to create a positive feedback mechanism which helped sustain the event and the magnificent streak lengths. Aside from an obviously narrow thermal window of opportunity, similarly optimal ice nuclei particle densities and perhaps even stratification were also likely in place. A lack of appreciable vertical wind shear limited the effects of dry air entrainment so as to even further prolong the lifetimes of the falling ice particles.

The irony of fallstreak observations, however, is that for any ground observer to see them there can be no lower-level cloud to block the view. A subtle, yet significant factor in this event was the detachment of the boundary layer regime from upper levels. Intuitively, had no such delineation been present, the dynamic reflection of the advancing short-wave trough, perhaps propagating as low as the ground, could have induced additional ascent at even lower levels. From Figs. 2b and 3b, the air at lower levels, though absolutely stable, were near saturation (likely from the recent precipitation). Had such ascent somehow been present, it is likely that lower level clouds would have formed in response. Under such conditions, the fallstreaks would have never been seen from the ground. At higher altitudes, say in the midlatitudes, where dynamic mechanisms

responsible for cloud growth are understood to commonly detach from lower/moister levels (i.e., associated with jet streaks, etc.) optimal viewing conditions are more likely to occur. As a result, cirrus uncinus observations are commonly made (hence their colloquial reverence). Ultimately, however, this is not to say the sorts of clouds discussed here do not occur more frequently, just simply out of sight of any ground observers.

Therefore, we conclude that these observations were quite fortuitous and notable, thus concurring with the opinion of Atlas (2001). However, this may ultimately apply only to the likelihood of such clouds forming in the midlatitudes. We cautiously remark that MPL observations from an ARM facility situated along the North Slope of Alaska, near Barrow, have captured multiple SLW/fallstreak formations in a five-year span of data collection. They have most typically formed in response to radiative cooling and thermally driven ascent (> 0.5 m/s as measured by an on-site 95 GHz cloud radar instrument) near the top of the local marine boundary layer at temperatures similar to those reported here (~ -25° C) [*Wang et al.*, 2003]. The lead author also recently made a visual observation of such clouds outside of Fairbanks, in the interior portion of Alaska. Given that optimal temperatures are much more common at lower altitudes above ground, lessening the need for lower cloud suppression and increasing the potential for suitable airborne nuclei from terrestrial sources, such clouds may ultimately be much more frequently observed in the polar regions. In any event, our interest in this case came from the historical veneration given to traditional uncinus fallstreaks and the unique thermodynamic structure that led to these anomalous observations. It is unfortunate that there was no sunlight around for anyone to enjoy and/or further document the sight.

ACKNOWLEDGEMENTS

The authors wish to thank Kenneth Sassen, Zhien Wang and William D. Hart for their comments and suggestions. This research was funded by the MPLNET project through the National Aeronautics and Space Administration (NASA) Earth Observing System and Sensor Intercomparison Biosphere program, the NASA Atmospheric Radiation Sciences program, and the Office of Biological and Environment Research of the U.S. Department of Energy as part of the Atmospheric Radiation Measurement Program (Ferrare). Atmospheric Radiation Measurement program data are available via the World Wide Web[3].

REFERENCES

Atlas, D., Fallstreaks and their parent generators, *Bull. Amer. Meteorol. Soc.*, **82,** 477-480, 2001.

Campbell, J.R., D.L. Hlavka, E.J. Welton, C.J. Flynn, D.D. Turner, J.D. Spinhirne, V.S. Scott, and I.H. Hwang, Full-time, eye-safe cloud and aerosol lidar observation at Atmospheric Radiation Measurement program sites: Instruments and data processing, *J. Atmos. Oceanic. Technol.*, **32,** 439-452, 2002.

Goldsmith, J.E.M., F.H. Blair, S.E. Bisson, D.D. Turner, Turn-key Raman lidar for profiling atmospheric water vapor, clouds and aerosols, *Appl. Opt.*, **37**(21), 4979-4990, 1998.

Heymsfield, A.J., Cirrus uncinus generating cells and the evolution of cirroform clouds. Part I. Aircraft measurements of the growth of the ice phase, *J. Atmos. Sci.,* **32,** 799-808, 1975a.

Heymsfield, A.J., Cirrus uncinus generating cells and the evolution of cirroform clouds. Part II, The structure and circulations of the cirrus uncinus generating head. *J. Atmos. Sci.*, **32,** 809-819, 1975b.

Heymsfield, A.J., Cirrus uncinus generating cells and the evolution of cirroform clouds. Part III. Numerical computations of the growth of the ice phase, *J. Atmos. Sci.,* **32,** 820-830, 1975c

Ludlam, F., The forms of ice clouds, *Quart. J. Roy. Meteor. Soc.*, **74,** 39-56, 1948.

Ludlam, F., The forms of ice clouds, II, *Quart. J. Roy. Meteor. Soc.*, **82,** 257-265, 1956.

[3] The ARM Data Archive may be accessed online at http://www.arm.gov.

Ludlam, F., Clouds and Storms, The Behavior and Effect of Water in the Atmosphere, The Pennsylvania State University Press, 404 pp, 1980.

Ralph, F.M., P.J. Newman, and T.L. Keller, Deep-tropospheric gravity waves created by leeside cold fronts, *J. Atmos. Sci.*, **56,** 2986-3009, 1999

Sassen, K., The polarization lidar technique for cloud research. A review and current assessment, *Bull. Amer. Meteorl. Soc.*, **72,** 1848-1866, 1991

Sassen, K., Cirrus: History and Perspective, in *"Cirrus"*, edited by D. K. Lynch et al., Oxford Press, 11-40, 2002.

Sassen, K, and G.C. Dodd, Homogeneous nucleation rate for highly supercooled cirrus cloud droplets, *J. Atmos. Sci.*, **45,** 1357-1369, 1988.

Sassen, K. and B.S. Cho, Subvisual-thin cirrus lidar dataset for satellite verification and climatological research. *J. Appl. Meteorol.*, **31,** 1275-1285, 1992.

Sassen, K., and S.K. Krueger, Toward an empirical definition of virga: Comments on "Is virga rain that evaporates before reaching the ground?", *Mon. Wea. Rev.*, **121,** 2426-2428, 1993

Spinhirne, J.D., Micro pulse lidar, *IEEE Trans. Geo. Rem. Sens.*, **31,** 48-55, 1993.

Spinhirne, J.D., W.D. Hart, and D.P. Duda, Evolution of the morphology and microphysics of contrail cirrus from airborne remote sensing, *Geophys. Res. Lett.*, **25,** 1153-1156, 1998

Stokes, G.M., and S.E. Schwartz, The Atmospheric Radiation Measurement (ARM) program: Programmatic background and design of the cloud and radiation testbed, *Bull. Amer. Meteorol. Soc.*, **75,** 1201-1221, 1994.

Turner, D.D., W.F. Feltz, and R.A. Ferrare, Continuous water vapor profiles from operational ground-based active and passive remote sensors, *Bull. Amer. Meteorol. Soc.*, **81,** 1301-1317, 2000.

Turner, D.D., R.A. Ferrare, L.A. Heilman, W.F. Feltz, and T. Tooman, Automated retrievals of aerosol extinction and backscatter coefficient profiles from a Raman lidar, *J. Atmos. Oceanic Technol.*, **19,** 37-50, 2002.

Worthington, R.M., An explanation for some fall streak clouds, *Annales Geophysicae*, **20,** 711-715, 2002

Wang, Z., K. Sassen, D.N. Whiteman, and B.B. Demoz, Studying altocumulus with virga using ground-based active and passive remote sensors, *J. Appl. Meteorol.*, submitted, 2003.

Figure Captions

Figure 1. MPL normalized relative backscatter (counts*km^2/μs*μm) from the ARM Southern Great Plains Central Facility for 31 December 2001 between 0000 – 1200 UTC.

Figure 2. CART Raman Lidar linear depolarization ratios (top) and derived relative humidities (with respect to water; bottom) from the ARM Southern Great Plains Central Facility for 31 December 2001 between 0000 – 1200 UTC.

Figure 3. Rawinsonde profiles from the ARM CART central facility in Oklahoma for December 31, 2001. Upper panel are potential temperature profiles at 0000, 0600 and 1200 UTC, progressively offset by 20 K (0000 UTC profile on left) with isentropic analysis at 1 K intervals. Lower panel is contour analysis of relative humidity (RH) with respect to liquid at temperatures warmer than 0°C, with respect to ice at temperature colder than -20°C, and linearly interpolated between these in the intervening region. Height is relative to mean sea level.

Figure 4. Temperature (heavy) and relative humidity (RH) with respect to water (thin) profiles at 0600 (solid) and 1200 (dashed) UTC. The profile of RH with respect to ice at 0600 UTC is also shown. Height is relative to mean sea level.

Figure 5. GOES-8 10.7 μm infrared and 6.8 μm water vapor imagery centered over the SGP CART domain from 0000 (a, e), 0300 (b, f), 0600 (c, g) and 0900 (d, h) UTC respectively. The Central Facility is denoted with a white dot in each still.

Figure 6. NOAA Profiler Network vertical velocity (m/s) data from the Vici, Oklahoma 404 MHz Doppler wind profiler between 2100 UTC 30 December – 0900 UTC 31 December. Positive values are toward the instrument, and therefore indicative of fallstreaks overhead.

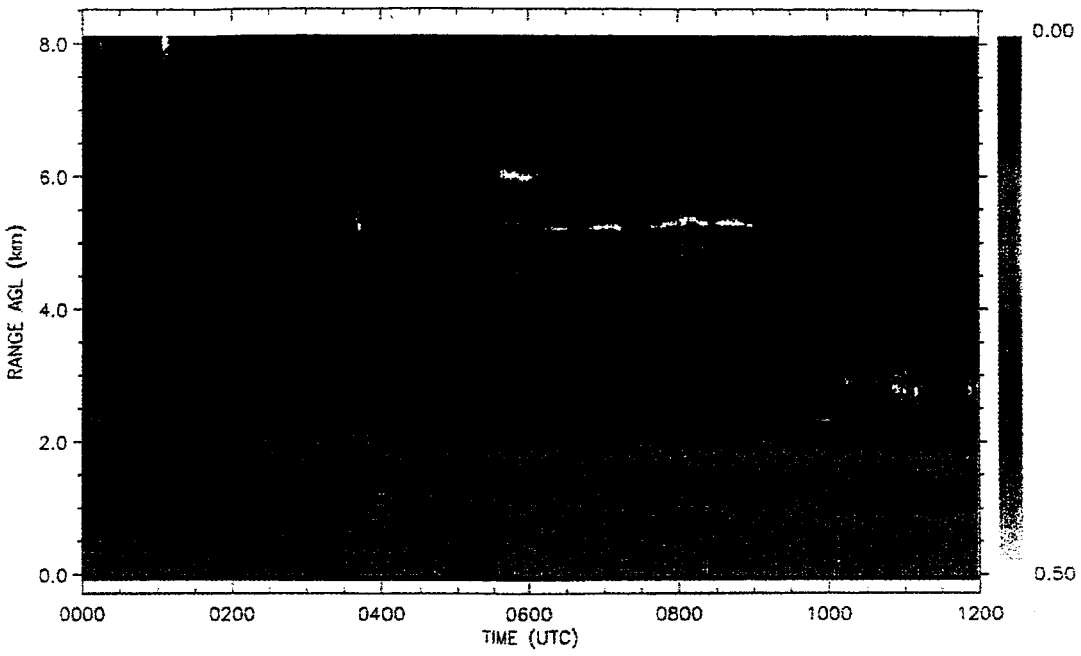
8.0
6.0
4.0
2.0
0.0
RANGE AGL (km)
0000
0200
0400
0600
0800
1000
1200
TIME (UTC)
0.00
0.50

Figure 1.

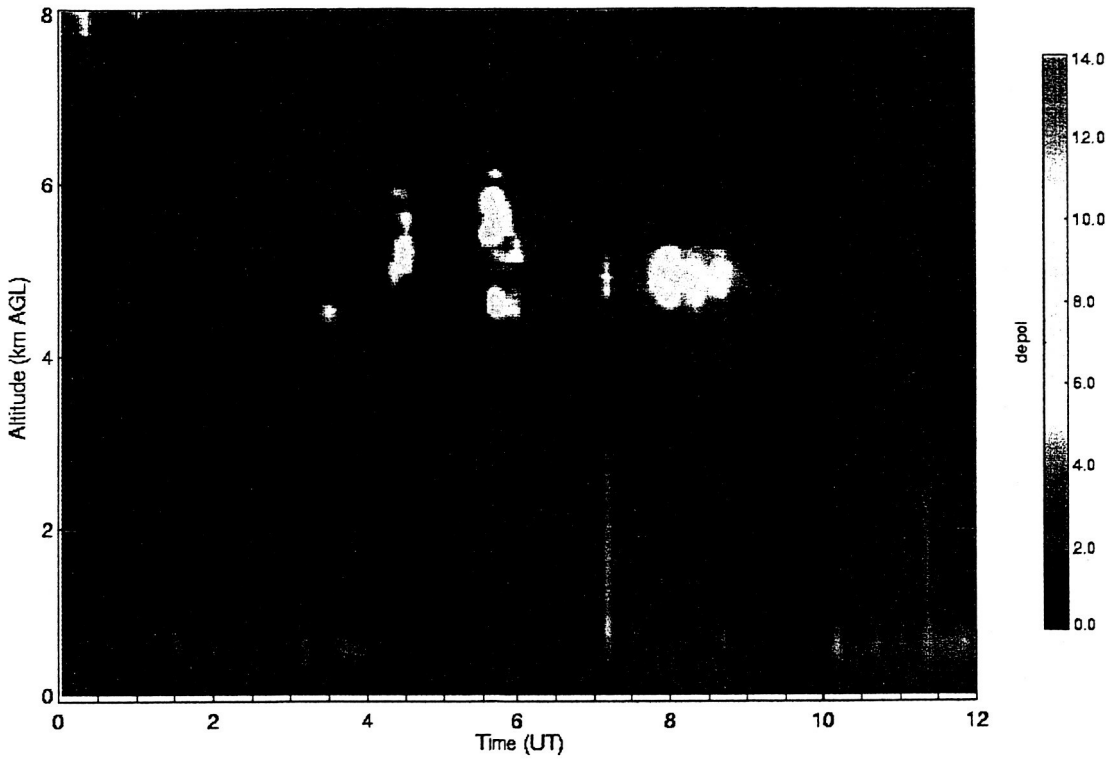
Altitude (km AGL)
Time (UT)
depol
0
2
4
6
8
10
12
14.0
12.0
10.0
8.0
6.0
4.0
2.0
0.0

(a)

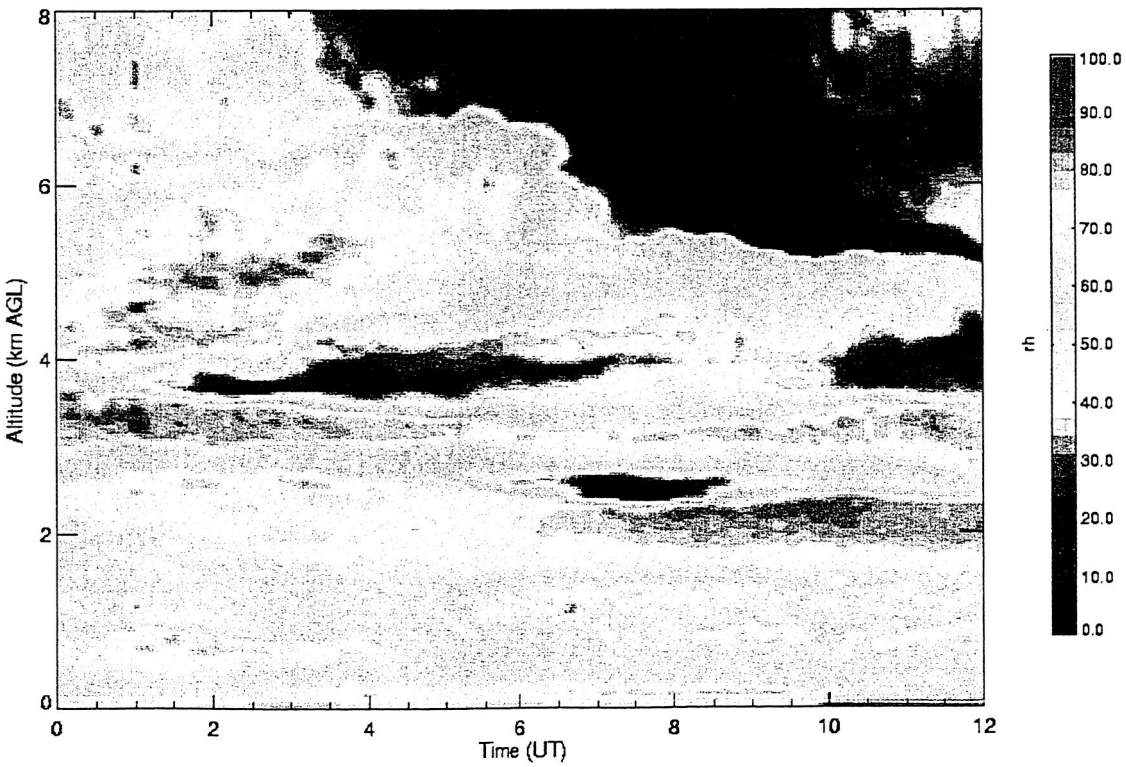
Altitude (km AGL)
Time (UT)
rh
0
2
4
6
8
10
12
100.0
90.0
80.0
70.0
60.0
50.0
40.0
30.0
20.0
10.0
0.0

(b)

Figure 2

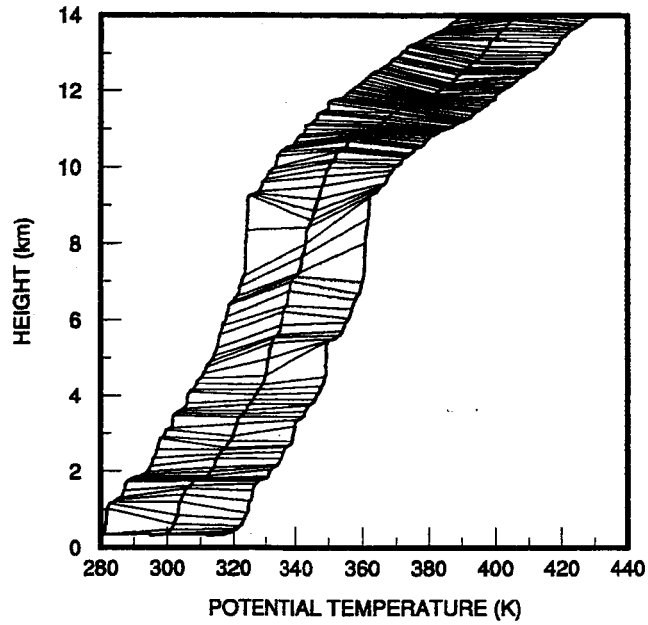
HEIGHT (km)
0
2
4
6
8
10
12
14
280
300
320
340
360
380
400
420
440
POTENTIAL TEMPERATURE (K)

(a)

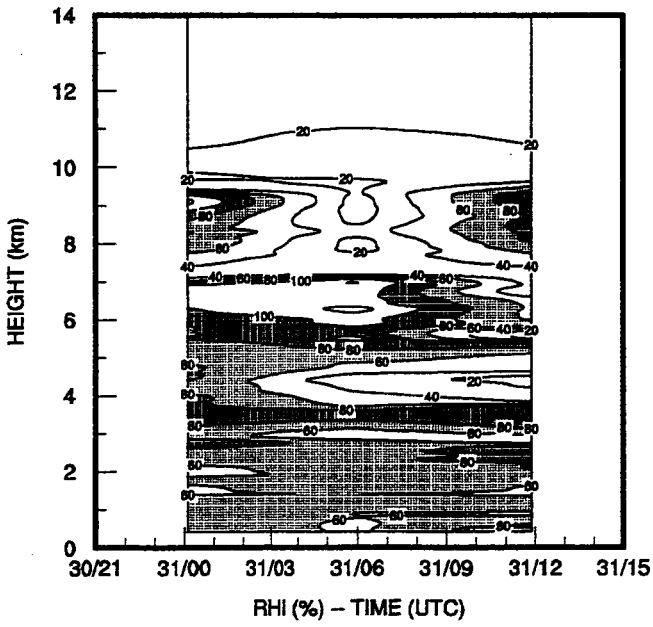
HEIGHT (km)
0
2
4
6
8
10
12
14
30/21
31/00
31/03
31/06
31/09
31/12
31/15
RHI (%) – TIME (UTC)

(b)

Figure 3

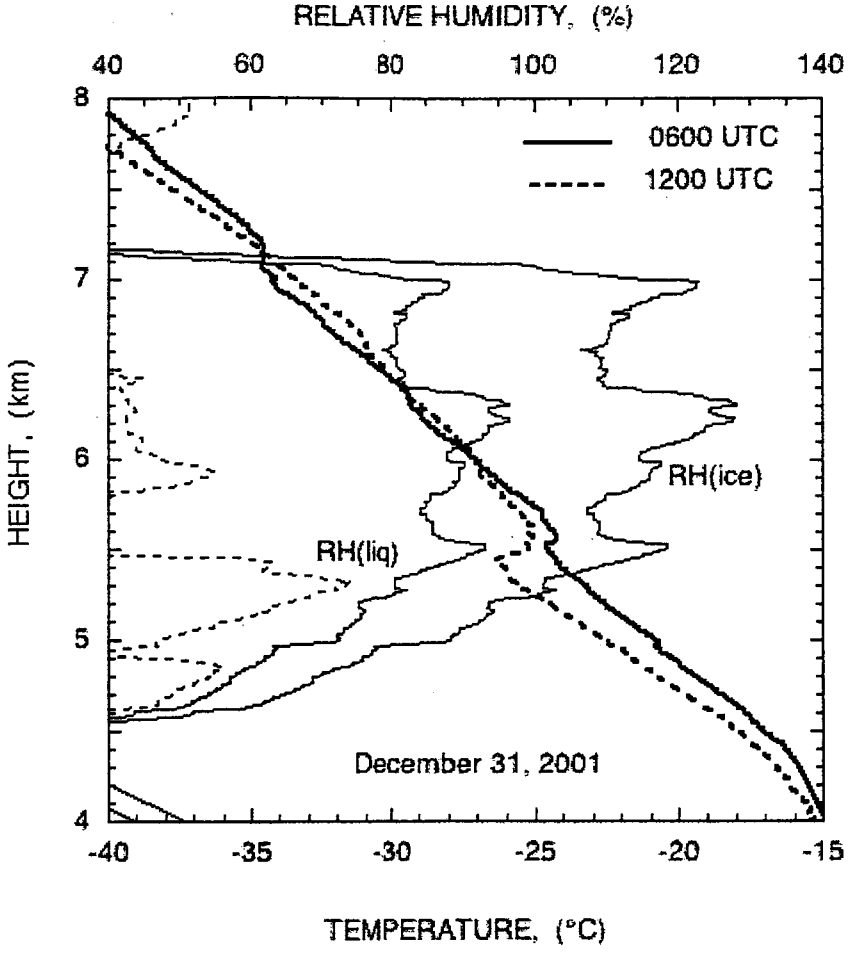
RELATIVE HUMIDITY, (%)
40
60
80
100
120
140
8
7
6
5
4
HEIGHT, (km)
0600 UTC
1200 UTC
RH(ice)
RH(liq)
December 31, 2001
-40
-35
-30
-25
-20
-15
TEMPERATURE, (°C)

Figure 4

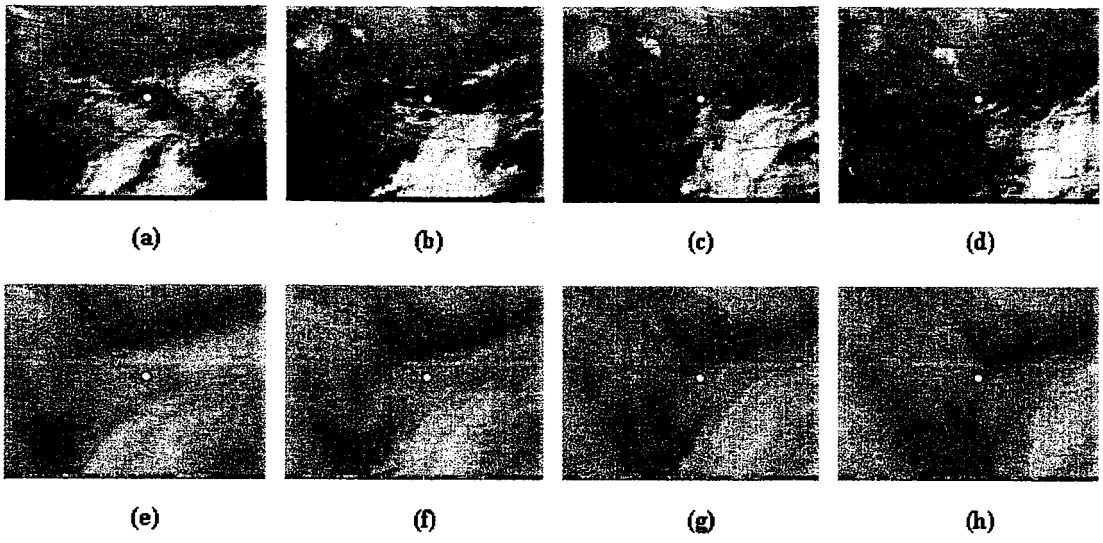

Figure 5

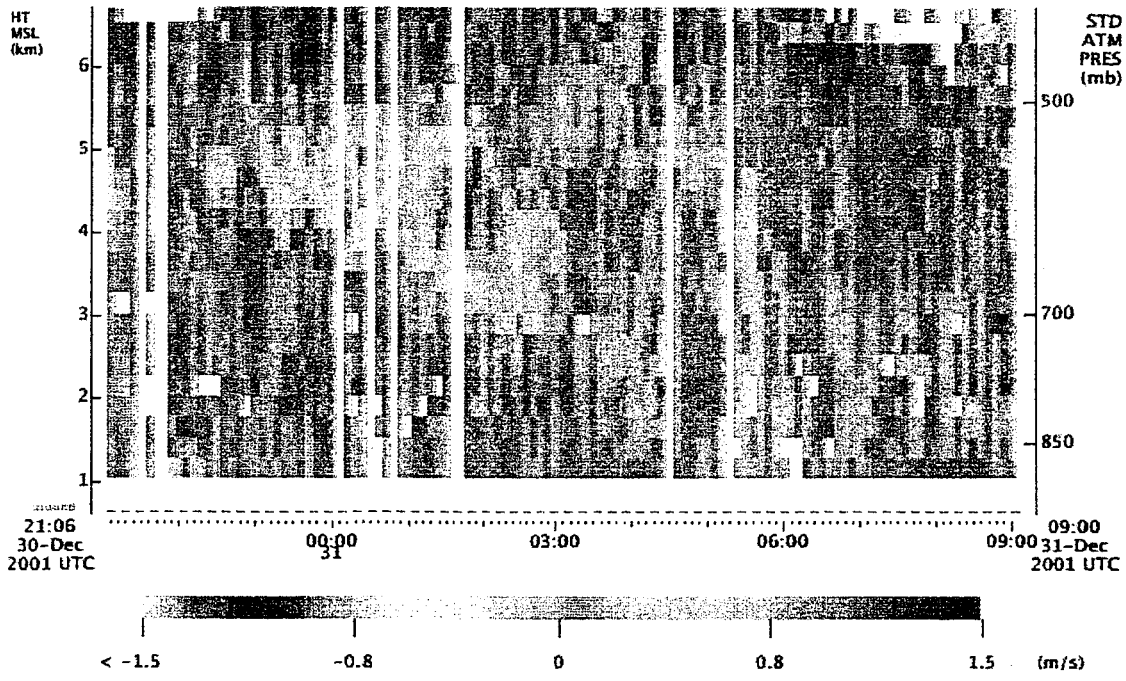
HT
MSL
(km)
6
5
4
3
2
1
STD
ATM
PRES
(mb)
500
700
850
21:06
30-Dec
2001 UTC
00:00
31
03:00
06:00
09:00
09:00
31-Dec
2001 UTC
< -1.5
-0.8
0
0.8
1.5
(m/s)

Figure 6